The DOI for this manuscript is doi: 10.1175/JCLI-D-14-00726.1

Key Role of North Pacific Oscillation/West Pacific Pattern in Generating the Extreme 2013-2014 North American Winter

Stephen Baxter
NOAA/NWS/NCEP Climate Prediction Center

Sumant Nigam
University of Maryland, College Park

Corresponding author:
Sumant Nigam
Department of Atmospheric and Oceanic Science
3419 Computer and Space Science Building
University of Maryland, College Park, MD 20742-2425
E-mail: *nigam@umd.edu*

Abstract

The 2013-2014 boreal winter (December 2013 – February 2014) brought extended periods of anomalously cold weather to central and eastern North America. We show that a leading pattern of extratropical variability, whose sea-level pressure footprint is the North Pacific Oscillation and circulation footprint the West Pacific teleconnection – together, the NPO/WP – exhibited extreme and persistent amplitude in this winter. Reconstruction of the 850-hPa temperature, 200-hPa geopotential height, and precipitation reveals that the NPO/WP was the leading contributor to the winter climate anomaly over large swaths of North America. Our analysis, furthermore, indicates that NPO/WP variability explains the most variance of monthly winter temperature over central-eastern North America since, at least, 1979. Analysis of the NPO/WP related thermal advection provides physical insight on the generation of the cold temperature anomalies over North America. Although NPO/WP's origin/excitation remains to be elucidated, its concurrent links to tropical SSTs are tenuous. Our findings suggest that notable winter climate anomalies in the Pacific-North American sector need not originate, directly, from the Tropics. More broadly, the attribution of the severe 2013-2014 winter to the flexing of an extratropical variability pattern is cautionary given the propensity to implicate the Tropics, following several decades of focus on El Niño-Southern Oscillation and its regional and far-field impacts.

Introduction

The 2013-2014 winter (December 2013 – February 2014) was anomalously cold across large swaths of central-eastern North America. Multiple, intense cold snaps prompted prolonged media attention, sent energy prices skyward, and led to scientific hypotheses on the cause of an extreme regional winter season in an otherwise warming global climate (Palmer 2014, for example). A careful analysis of the established winter patterns of monthly atmospheric circulation variability and their near-surface temperature footprints attributes the 2013-2014 extreme winter across North America, largely, to the North Pacific Oscillation/West Pacific pattern (NPO/WP).

The NPO/WP acronym is used for North Pacific Oscillation (NPO) and the West Pacific (WP) teleconnection pattern. The North Pacific Oscillation, a north-south seesaw in winter sea-level pressure over the North Pacific on monthly (and shorter) timescales, was identified by Sir Gilbert Walker in 1924. The NPO was known to synoptic forecasters of the United States Weather Bureau as early as 1916 because of its significant influence on US winter weather. They noted that the oscillation phase with higher pressure over Alaska and lower pressure over Hawaii was linked with colder conditions over eastern North America, much as during the 2013-2014 winter. The WP pattern was defined by Wallace and Gutzler (1981) from teleconnection analysis of the mid-tropospheric geopotential height field in boreal winter. It consists of a north-south dipole over the western Pacific basin in the Northern Hemisphere. Later analysis showed the WP and NPO to be essentially the same variability, with the NPO being the sea-level pressure reflection of the WP geopotential height pattern (Wallace and Gutzler 1981; Nigam 2003; Linkin and Nigam 2008).

The NPO/WP variability pattern is the Pacific basin analog of the North Atlantic Oscillation (NAO; Nigam 2003). Both consist of a north-south dipole in sea level pressure and tropospheric height anomalies across their basins as well as latitudinal displacement of the climatological jet streams. Not surprisingly, each alters the storm tracks near and downstream of their centers of action, with the NAO impacts pronounced over far eastern North America and Europe, and the NPO/WP ones influential over northeastern Asia and North America. Large amplitude monthly and seasonal geopotential height anomalies resembling the WP pattern would thus be well-positioned to significantly impact the surface climate over North America – the case in 2013-2014 winter.

There is some recent literature that has related NPO variability to changes in central Pacific SSTs, namely, central Pacific El Niño events (DiLorenzo et al, 2013; Furtado et al. 2012), mostly on decadal time scales. Our analysis suggests that links on monthly and seasonal timescales are tenuous at best, as the SST and outgoing longwave radiation (OLR, used as a proxy for tropical convection) footprints of the NPO/WP as revealed here are weak (correlations of ~0.2 or less, not shown).

Another variability pattern of some significance this past winter is the Tropical-Northern Hemisphere (TNH) pattern. The TNH was identified by Mo and Livezy (1986), and was believed to be related to El Niño Southern Oscillation (ENSO) variability. Nigam (2003) however showed ENSO's extratropical winter response to be distinct from the TNH pattern. Rotated empirical orthogonal function (EOF) analysis of 200-hPa heights (as in this study, and Nigam 2003) yields two patterns related to SST variability in the tropical Pacific: *a)* a height response in the western hemisphere extratropics and global tropics with little subseasonal variability (ENSO's classic

winter season response), and *b)* a more extratropically confined response exhibiting greater month-to-month variability (TNH-like pattern).

The objective of this analysis is quantitative attribution of the 2013-2014 winter circulation and temperature anomalies over North America. The identification of the key building blocks and related reconstruction provide mechanistic insight on the development of phenomenally cold winter temperatures. Our implication of NPO/WP variability – currently viewed as a mode of internal variability – for the highly abnormal 2013-2014 winter has potentially wide-reaching implications for subseasonal-to-seasonal climate predictability. The data sets and analysis methods are briefly discussed next while the obtained findings and its implications follow in later sections.

Data and Methods

The analysis draws on the Climate Forecast System Reanalysis (CFSR; Saha et al. 2010) for 200-hPa geopotential height (Z_{200}), 850-hPa temperature (T_{850}) and winds, and 700-hPa vertical velocity (ω_{700}), all at monthly resolution and on a 2.5° global grid. The pentad (i.e., 5-day averaged) T_{850} and 200-hPa streamfunction from the CFSR are used to assess subseasonal variability. The precipitation data (on a 0.5° continental grid) is obtained from NOAA-Climate Prediction Center's unified gauge-based dataset (Chen et al., 2002). The January 1979 – February 2014 period is analyzed, with anomalies defined with respect to the 1981-2010 climatology, as in NOAA's Climate Diagnostic Bulletin (hereafter, CDB; monthly archive is online).

The NPO/WP pattern is obtained alongside other variability patterns in a rotated EOF analysis of monthly, winter (December, January, February) Z_{200} anomalies in the Northern Hemisphere. The leading eight patterns are rotated using the varimax technique, as in Nigam

131 (2003). In this analysis, the NPO/WP emerges as the third-leading pattern, explaining ~11% of
132 the monthly winter variance, after the NAO (~17%) and ENSO response (~13%) patterns. The
133 THN is the fifth-leading mode in this analysis, explaining ~6% of the variance.

134 To assess the contribution of the NPO/WP, TNH, and other variability patterns to the
135 extreme 2013-2014 winter, the T_{850}, Z_{200}, and precipitation (and ω_{700}) anomalies are
136 reconstructed. Multiplication of each rotated EOF pattern (spatial) with its principal component
137 (time-varying) value for the target month, and summing the various EOF contributions yields the
138 reconstructed signal; the principal components (PCs) are orthogonal, facilitating reconstruction.
139 The December 2013, and January and February 2014 reconstructions were averaged to produce
140 the 2013-2014 winter season anomalies, discussed in the next section.

141 To assess subseasonal variability, a similar analysis is performed on the pentad 200-hPa
142 streamfunction (ψ_{200}) anomalies; streamfunction is a preferred variable for analysis of tropical-
143 extratropical interaction. Following Baxter and Nigam (2013), an extended, rotated EOF analysis
144 is conducted to extract the subseasonal modes of spatiotemporal variability. Analysis of ψ_{200}
145 yields a clearer identification of the Madden-Julian Oscillation's (MJO) extratropical response,
146 precluding its aliasing onto the extratropical variability patterns. The 120-day running mean
147 anomaly is removed from data prior to analysis, to filter out interannual variability. The data are
148 'extended' using a five-pentad sampling window. In this analysis, NPO/WP emerges as the
149 fourth-leading mode, behind two modes that capture the time-lagged MJO response, and the
150 Pacific–North American (PNA) pattern.

151 While the reconstructions themselves are informative, mechanistic links between the
152 NPO/WP circulation and temperature anomalies over North America are also investigated. To

this end, the various terms constituting thermal advection are evaluated for the 2013-2014 winter season:

$$(A)\ -\boldsymbol{V}_{850}^{NPO/WP} \cdot \boldsymbol{\nabla} T_{850}^{C}$$

$$(B)\ -\boldsymbol{V}_{850}^{NPO/WP} \cdot \boldsymbol{\nabla} T_{850}^{NPO/WP*}$$

$$(C)\ -\boldsymbol{V}_{850}^{C} \cdot \boldsymbol{\nabla} T_{850}^{NPO/WP*}$$

Term (A) constitutes the advection of climatological T_{850} by the NPO/WP contribution to the 850-hPa wind. Term (B) represents a quasi-nonlinear advection – of the *first-order* NPO/WP temperature signal ($T^{NPO/WP*}$) by the NPO/WP related winds. As the *observed* NPO/WP T_{850} anomaly is the reconstruction target, it cannot be used here. The first-order temperature signal is estimated, indirectly, from Term A using the thermal damping from synoptic transient eddies (Lau 1979).[1] Finally, term (C) constitutes the advection of the first-order NPO/WP temperature signal by the climatological 850-hPa wind.

Results

The 2013-2014 winter was characterized by significantly below-normal temperatures across much of North America. The NPO/WP principal component was strongly negative, consistent with higher pressure/heights over Alaska and colder-than-normal temperatures over central-eastern North America. The NPO/WP PC averaged over the three winter months exhibited the most negative seasonal value over the entire analysis period (cf. Fig. 4b). Figure 1a shows the observed T_{850} anomalies, with temperatures as cold as −7°C centered southwest of Hudson Bay. The cold temperatures extend from northwestern Canada southeastward to well-

[1] The first-order NPO/WP temperature signal $\boldsymbol{T}_{\boldsymbol{850}}^{\boldsymbol{NPO/WP*}}$ is estimated as $-\boldsymbol{V}_{850}^{NPO/WP} \cdot \boldsymbol{\nabla} T_{850}^{C} \approx -\gamma\, \boldsymbol{T}_{\boldsymbol{850}}^{\boldsymbol{NPO/WP*}}$ where the right hand side represents thermal (Newtonian) damping of lower tropospheric temperature by synoptic transients. γ is taken as $(3\ \text{days})^{-1}$ following Lau (1979, Table-I).

populated parts of the central-eastern United States. Above-normal T_{850} was observed over much of Alaska, US west coast, and southwestern U.S. The structure and magnitude of the observed anomalies are closely reconstructed (Fig. 1b) using PCs of the NPO/WP, NAO, TNH, and East Atlantic (EA, Wallace and Gutzler 1981) patterns; panels *c-f* show the individual contributions. The NPO/WP contribution clearly resembles the observed anomaly most closely, followed distantly by the TNH. The red outlined box in the panels marks a region of the Northern Plains (40-55N, 100-80W) whose area-averaged T_{850} anomalies are used in time series analyses. The region was selected due to its proximity to the core of the cold anomaly and the populated areas in the north central-eastern quadrant of the continent.

Figure 2 displays the 200-hPa geopotential height anomaly for this winter. As in Figure 1, the reconstructed Z_{200} anomaly is displayed alongside the observed (CFSR) one, along with the individual contributions. As with T_{850}, the NPO/WP's Z_{200} contribution is dominant over North America and closely similar to the observed anomaly there. Figure 2e indicates that TNH was also a contributor over North America but with significantly smaller amplitudes than NPO/WP. It is worth noting that both NAO and EA patterns were also active, with strong projections on the observed T_{850} and Z_{200} anomalies but in the downstream Atlantic and European sectors.

While bitterly cold temperatures in the central-eastern United States defined the 2013-2014 winter, the precipitation anomaly was also notable. Most significant, perhaps, was the anomalously dry winter over the West Coast, especially California (Fig. 3a). The TNH and NPO/WP contributions can explain most of the observed precipitation deficits extending from the Alaskan panhandle to southern California (Figs. 3*a*, *c*, and *e*). In fact, from central California to most of the Alaskan panhandle, those two patterns account for over 75% of the observed precipitation deficit (in some cases the reconstruction yields a deficit higher than observed).

198 Over southern California and the Desert Southwest, the reconstruction from the TNH and
199 NPO/WP generally explains 50-75% of the observed precipitation anomalies. Of the two
200 patterns, the TNH explains more variability over California, a region of intense study given the
201 multiyear drought that has impacted that region.

202 The precipitation signals are consistent with the observed and reconstructed 700-hPa
203 vertical velocity anomalies across western North America (Fig.3, right panels). The NPO/WP
204 explains some of the wet signal also along the eastern seaboard, though other variability is
205 clearly more important in that region.

206 In order to place the 2013-2014 winter in historical context, the time series of the area-
207 averaged T_{850} anomalies over the Northern Plains (red box, Fig. 1) is examined in Figure 4b,
208 which also shows the standardized NPO/WP principal component; the two are correlated at 0.69,
209 a high value. The winter exhibiting the most negative seasonal T_{850} anomaly (i.e., most
210 persistently cold) is this past one (2013-2014), when the NPO/WP PCs are also most negative.
211 The TNH pattern also contributed to the recent record cold winter (cf. Fig. 1e) but its
212 contribution is secondary to NPO/WP's. The relative contribution of the two patterns in other
213 extreme winters (when regional T_{850} exceeded ± 1 standard deviation) is examined via a scatter
214 plot of the two PCs in Figure 4c. It is noteworthy that every winter month satisfying the
215 threshold for cold (warm) extremeness had a negative (positive) PC value but only in case of the
216 NPO/WP. The TNH PC was not found as tightly correlated as it exhibits positive values in both
217 cold and warm winters, albeit more often in the cold ones.

218 The subseasonal variability in the extreme 2013-2014 winter over the Northern Plains is
219 briefly examined in Figure 4a. The pentad T_{850} anomaly index (standardized) co-varies with the
220 pentad NPO/WP principal component, with the exception of the last few pentads. Over this

extreme winter, the two pentad indices are correlated at 0.56;[2] the correlation is 0.45 over all analyzed winters (1979-2014). The pentad correlation for this winter and across all winters is impressive, highlighting the preeminence of the NPO/WP pattern in influencing the winter surface climate over Northern Plains, even on subseasonal timescales. Correlations in the 0.4-0.6 range indicate that the NPO/WP influence is far from complete: Subseasonally, this is reflected in the near-zero principal component values of NPO/WP during mid-January of 2014 (cf. Fig. 4a). The significant contribution of TNH variability on monthly timescales was noted earlier.

The observationally rooted analysis presented above attributes the extreme 2013-2014 winter temperatures over North America to NPO/WP variability. The statistical attribution is provided a mechanistic underpinning in this section which elaborates on the temperature advection processes, in particular the phenomenal cold advection experienced by the Northern Plains and the central-eastern United States. The advection of climatological T_{850} can account for the spatial structure of NPO/WP-related anomalies east of the Rocky Mountains, but not its magnitude (Fig. 5b). Using this field (Fig. 5b) and a 3-day Newtonian damping (to represent thermal damping by synoptic transient eddies), NPO/WP's first-order T_{850} signal is constructed (see Footnote 2; not shown). The advection of this first-order T_{850} signal by the climatological 850-hPa wind field (Fig. 5d) contributes significantly to the *total* NPO/WP temperature advection (the sum of panels *b*-*d*, shown in panel *a*). In fact, the temperature anomaly resulting from the total NPO/WP advection (with 3-day thermal damping) is larger than the NPO/WP T_{850} reconstruction itself. Clearly other terms in the thermodynamic energy equation, such as the

[2] A higher pentad correlation is obtained with T_{850} leading by 1-pentad. This results from the retrogression of the NPO/WP pattern whose North American center attains peak amplitude in advance of other regions. The NPO/WP PC is, of course, keyed to the overall mature structure. The T_{850} lead over the Northern Plains is, by no means, indicative of causality; see Figure 5.

adiabatic and latent heating, are important. The quasi-nonlinear advection term (Fig. 5c), however, is mostly unimportant relative to the other two advection terms.

Concluding remarks

A key element of the scientific method is seeking support for the proposed hypothesis by expanding the inquiry domain. After attributing the anomalously cold 2013-2014 North American winter (and drought over the Pacific-Northwest) to the heightened negative phase of the NPO/WP pattern, we inquire if NPO/WP variability can be implicated in the generation of unusually warm North American winters as well. In March 2012, large swaths of central-eastern North America were warmer than normal by as much as 5°C and the Pacific Northwest wetter by 25-50% (CDB, Fig. E6). Support for a prominent role of the NPO/WP (positive phase) in this warming episode follows from the large spatial anomaly correlation (-0.66) of this month's T_{850} anomalies with the NPO/WP T_{850} regression pattern (Fig. 1c), footprint of the precipitation anomaly, and the striking similarity of the March 2012 Z_{300} anomalies (CDB, Fig. S1) with the NPO/WP's (Fig. 2c but for the sign). The projection of the March 2012 Z_{200} anomalies onto the wintertime NPO/WP loading pattern was 1.24, a significantly positive value.

A pertinent question in context of this attribution is the longevity of the NPO/WP pattern. A monthly analysis is likely to be too coarse for this estimation but a pentad-resolution spatiotemporal analysis (e.g., Baxter and Nigam 2013) should suffice. This analysis yields 25 days as the duration timescale of a NPO/WP episode, based on the autocorrelation fall-off to e^{-1}.

The origin of the NPO/WP remains enigmatic: Concurrent links to the tropical SSTs are tenuous but linkage with extratropical SSTs (especially in the Gulf of Alaska) is strong in the monthly analysis (Nigam and Baxter 2014, Fig. 9c); additional analysis, including SST-leading links, is warranted given the prominent role of NPO/WP in influencing North America's winter

hydroclimate. Interestingly, the Gulf of Alaska SSTs were notably positive this past winter (CDB, Fig. T18; Washington Post 2014), when the NPO/WP was strongly negative (cf. Fig. 4a) and Pacific storm tracks southward of their normal location (CDB, Fig. E13).

Finally, this analysis cautions against succumbing to the post-1980/90s temptation of ascribing various extratropical anomalies in the Pacific/North American sector to ENSO – a favorite go-to mechanism because a causal inference is drawable, unlike the extratropical rooted teleconnections whose origin/mechanisms remain to be elucidated. For example, a recent NOAA report on the causes and predictability of the California drought (Seager et al. 2014) utilizes climate modeling to suggest that the persistent, amplified circulation pattern over North America (the immediate synoptic-climate cause of the drought over California) may have been forced in part by the anomalously warm SSTs in the tropical West Pacific and related tropical convection. An influential role of these SSTs on North American winter climate is also highlighted in another recent study (Hartmann 2015). Neither of these studies, however, provides process-level observational support (e.g., through OLR or diabatic heating analysis) for the posited causal link. The present study, with its emphasis on internal midlatitude variability, suggests that any tropical forcing is substantially weaker than the role of the NPO/WP, whose origin and evolution remain largely unknown, especially on seasonal timescales. This lack of mechanistic underpinning however does not make these teleconnections any less relevant in attribution analysis. Instead, a concerted research focus on their excitation, evolution, and longevity is warranted.

References

- Baxter, S. & Nigam, S. A Subseasonal Teleconnection Analysis: PNA Development and Its Relationship to the NAO. *Journal of Climate*, **26**, 6733-6741, doi:10.1175/JCLI-D-12-00426.1 (2013).
- Chen, M., P. Xie, J. E. Janowiak, and P. A. Arkin (2002), Global land precipitation: A 50-year monthly analysis based on gauge observations, J. Hydrometeorol., **3**, 249–266.
- Climate Diagnostics Bulletin Archive. From http://www.cpc.ncep.noaa.gov/products/CDB/CDB_Archive_pdf/pdf_CDB_archive.shtml
- Di Lorenzo, E., et al., 2013: Synthesis of Pacific Ocean climate and ecosystem dynamics. *Oceanography* **26**(4):68-81. doi:10.5670/oceanog.2013.76
- Furtado, J. et al.: 2012. Linkages between the North Pacific Oscillation and central tropical Pacific SSTs at low frequencies. *Climate Dynamics* **39**: 2833-2846.
- Hartmann, D. L., 2015: Pacific Sea Surface Temperature and the Winter of 2014. Geophys. Res. Lett.**43,** DOI: 10.1002/2015GL063083.
- Izadi, E. "The Gulf of Alaska is unusually warm, and weird fish are showing up." *Washington Post*, 15 Sep 2014. Web.
- Lau, N-C. The Observed Structure of Tropospheric Stationary Waves and the Local Balances of Vorticity and Heat. *Journal of the Atmospheric Sciences*, **36**, 996-1016, doi:10.1175/1520-0469(1979)036<1844:OTDOHT>2.0.CO;2 (1979).
- Linkin, M. E., and S. Nigam, 2008: The North Pacific Oscillation--West Pacific teleconnection pattern: Mature-phase structure and winter impacts. J. Climate, **21**, 1979-1997.

- Mo, K. & Livezey, R. Tropical-Extratropical Geopotential Height Teleconnections During the Northern Hemisphere Winter. *Monthly Weather Review,* **114**, 2488-2515, doi:10.1175/1520-0493(1986)114<2488:TEGHTD>2.0.CO;2 (1986).
- Nigam, S. and S.Baxter (2014): Teleconnections. *Encyclopedia of Atmospheric Sciences (2nd edition)*; Editors: G. North, Academic Press, Elsevier Science, London (in press).
- Nigam, S., 2003: Teleconnections. *Encyclopedia of Atmospheric Sciences*; Editors: J.R. Holton, J.A. Pyle & J.A. Curry; Academic Press, Elsevier Science, London, 2243-2269.
- Palmer, T. Record-breaking Winters and Global Climate Change. *Science,* **344**, 803-804, doi:10.1126/science.1255147 (2014).
- Rogers, J. C., 1981: The North Pacific Oscillation. *J. Climatology*., **1**, 39-57.
- Saha, S. *et al.* The NCEP Climate Forecast System Reanalysis. *Bulletin of the American Meteorological Society,* **91**, 1015-1057, doi:10.1175/2010BAMS3001.1 (2010).
- Seager, R., and Coauthors, 2014: Causes and Predictability of the 2011-14 California Drought, doi:10.7289/V7258K7771F, 40pp.
- Walker, G. T. 1924. Correlation in seasonal variations in weather IX: A further study of world weather. Mem. Indian Meteor. Dep. 24. 275–332.
- Wallace, J. M. and D. S. Gutzler, 1981: Teleconnections in the geopotential height field during the Northern Hemisphere winter. Mon. Wea. Rev.,**109**, 784–812.

Figure Captions

Figure 1: 850-hPa temperature anomalies for December 2013--February 2014, i.e., DJF 2013-14 winter: A) Observed. Panels *b-f* show T_{850} anomalies from a reconstruction based on principal components (PC) of the 200-hPa geopotential height (Φ_{200}) variability; see text for analysis details: B) From four pertinent modes; C) from NPO/WP; D) from NAO; E) from TNH; and F) from East Atlantic (EA) pattern. T_{850} anomalies are reconstructions by multiplying the Φ_{200} PC of each month by its regression pattern. The reconstructed winter month anomalies were then averaged to obtain the winter season (DJF) reconstruction. The contour interval and shading threshold is 0.5K. The red box (40-55N, 95-80W) marks the Great Plains averaging region for the T_{850} anomaly index discussed in subsequent analysis.

Figure 2: As in Figure 1, but for the 200-hPa geopotential height anomalies; contour interval and shading threshold is 15m. Principal components obtained from the variability analysis of this field are the basis for all reported reconstruction.

Figure 3: Precipitation and 700-hPa vertical velocity (W_{700}) anomalies during DJF2013-14: A) Observed precipitation anomaly, and its reconstruction from NPO/WP (C) and TNH (E) principal components. B) Observed W_{700} anomaly, and its reconstruction from the same principal components in D) and F), respectively. Contour interval and shading threshold is 0.25 mm/day for precipitation, and 1 cm/s for W_{700}.

Figure 4: Pentad (A) and monthly (B) distribution of the NPO/WP principal component and T_{850} over the Great Plains (marked box in Fig. 1); the upper panel focuses on recent winter (DJF 2013-14) while the middle one covers the entire analysis period winters (1979-2014). The 200-hPa winter geopotential height (streamfunction) variability during 1979-2014 utilized for the

seasonal (pentad) analysis, with correlation coefficients noted in the legend. (C) Scatter plot of the NPO/WP and TNH principal components from the 1979-2014 monthly analysis, when the T_{850} anomaly over the Great Plains exceed ±1 standard deviation. Blue (red) dots denote cold (warm) winter months.

Figure 5: Reconstructed 850-hPa thermal advection related to NPO/WP. (A) Total thermal advection constituting the sum of panels *b-d*. (B) Advection of climatological 850-hPa temperature by the NPO/WP related wind anomaly, i.e., $\{-\overrightarrow{V_a} \bullet \vec{\nabla} T_c\}_{850\ \mathrm{hPa}}$, where $\overrightarrow{V_a}$ is the anomaly attributed to the NPO/WP and T_c is the climatological temperature. (C) Quasi-nonlinear term, $\{-\overrightarrow{V_a} \bullet \vec{\nabla} T_{NPO/WP}\}_{850\ \mathrm{hPa}}$, where $\vec{\nabla} T_{NPO/WP}$ is derived from panel (B) using a 3-day thermal dissipation time scale (cf. Lau 1979, Table 1). (D) The advection of $T_{NPO/WP}$ by the climatological 850-hPa wind, $\{-\overrightarrow{V_c} \bullet \vec{\nabla} T_{NPO/WP}\}_{850\ \mathrm{hPa}}$. Contour interval and shading threshold is 3.86E-6 K/s, a value that yields ΔT=1.0K for a 3-day thermal dissipation time scale. Data are also subject to a nine-point smoother to improve figure clarity.

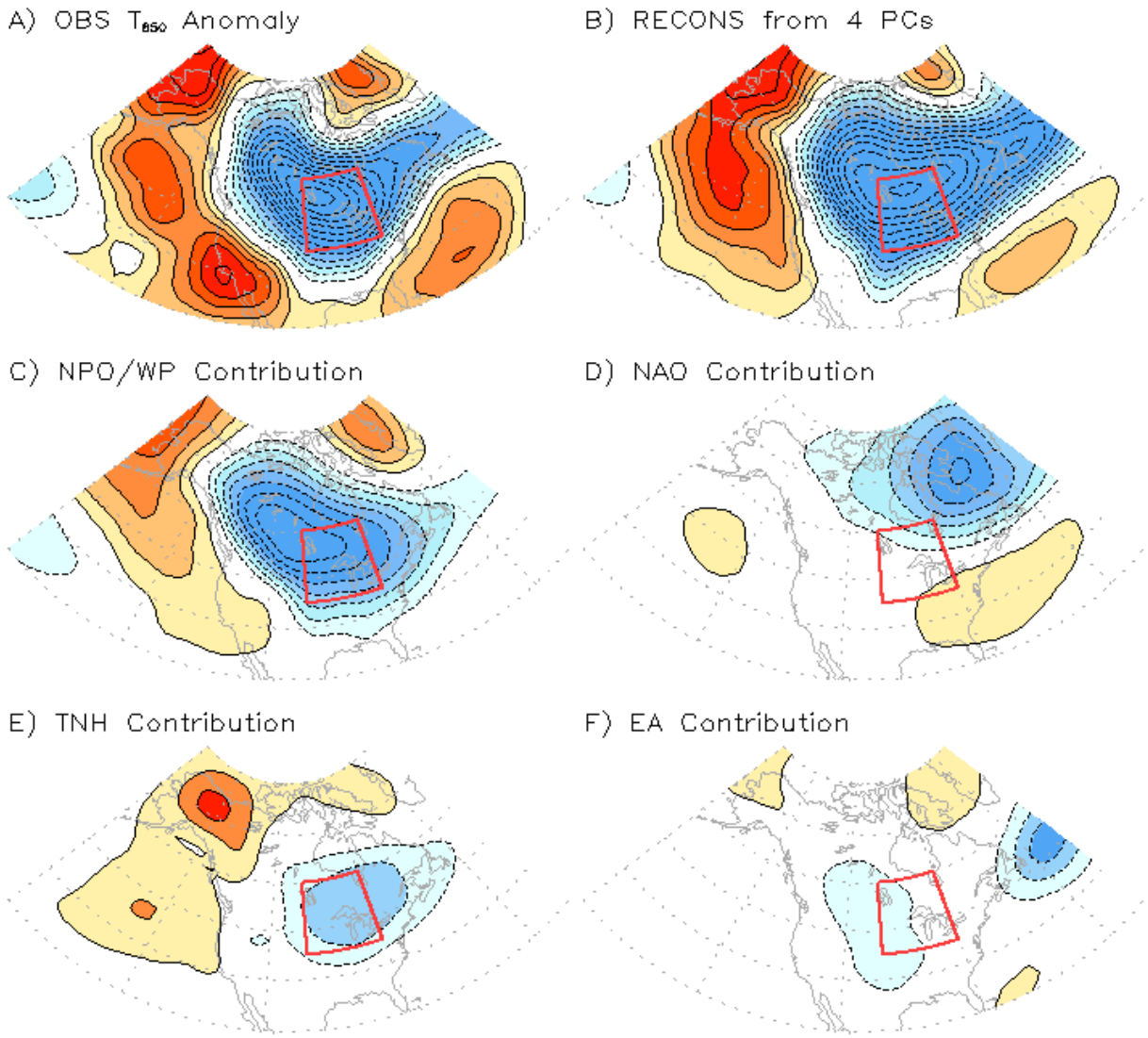

Figure 1. 850-hPa temperature anomalies for December 2013--February 2014, i.e., DJF 2013-14 winter: A) Observed. Panels *b-f* show T_{850} anomalies from a reconstruction based on principal components (PC) of the 200-hPa geopotential height (Φ_{200}) variability; see text for analysis details: B) From six pertinent modes; C) from NPO/WP; D) from NAO; E) from TNH; and F) from East Atlantic (EA) pattern. T_{850} anomalies are reconstructions by multiplying the Φ_{200} PC of each month by its regression pattern. The reconstructed winter month anomalies were then averaged to obtain the winter season (DJF) reconstruction. The contour interval and shading threshold is 0.5K. The red box (40-55N, 95-80W) marks the Great Plains averaging region for the T_{850} anomaly index discussed in subsequent analysis.

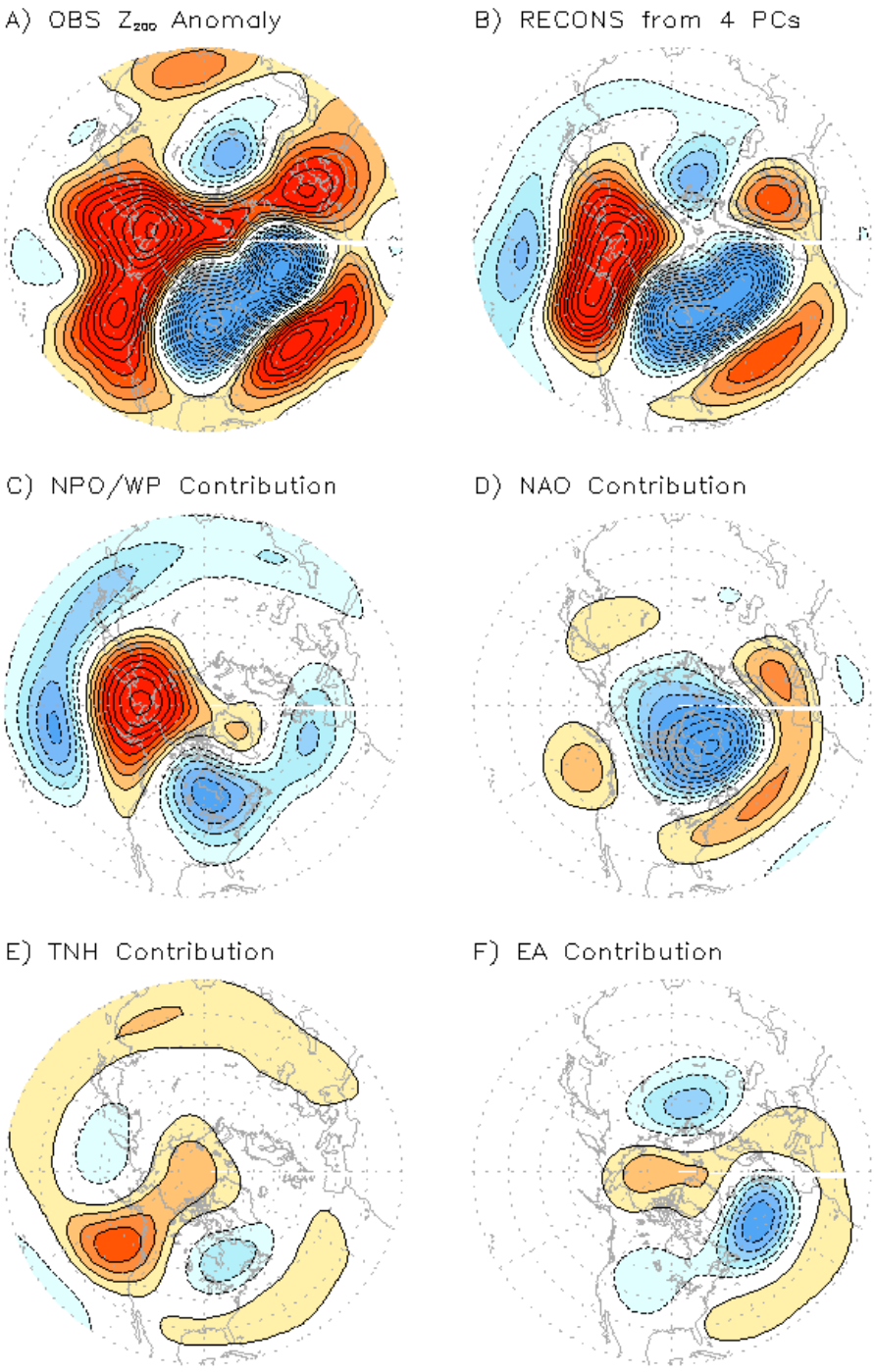

Figure 2. As in Figure 1, but for the 200-hPa geopotential height anomalies; contour interval and shading threshold is 15m. Principal components obtained from the variability analysis of this field are the basis for all reported reconstruction.

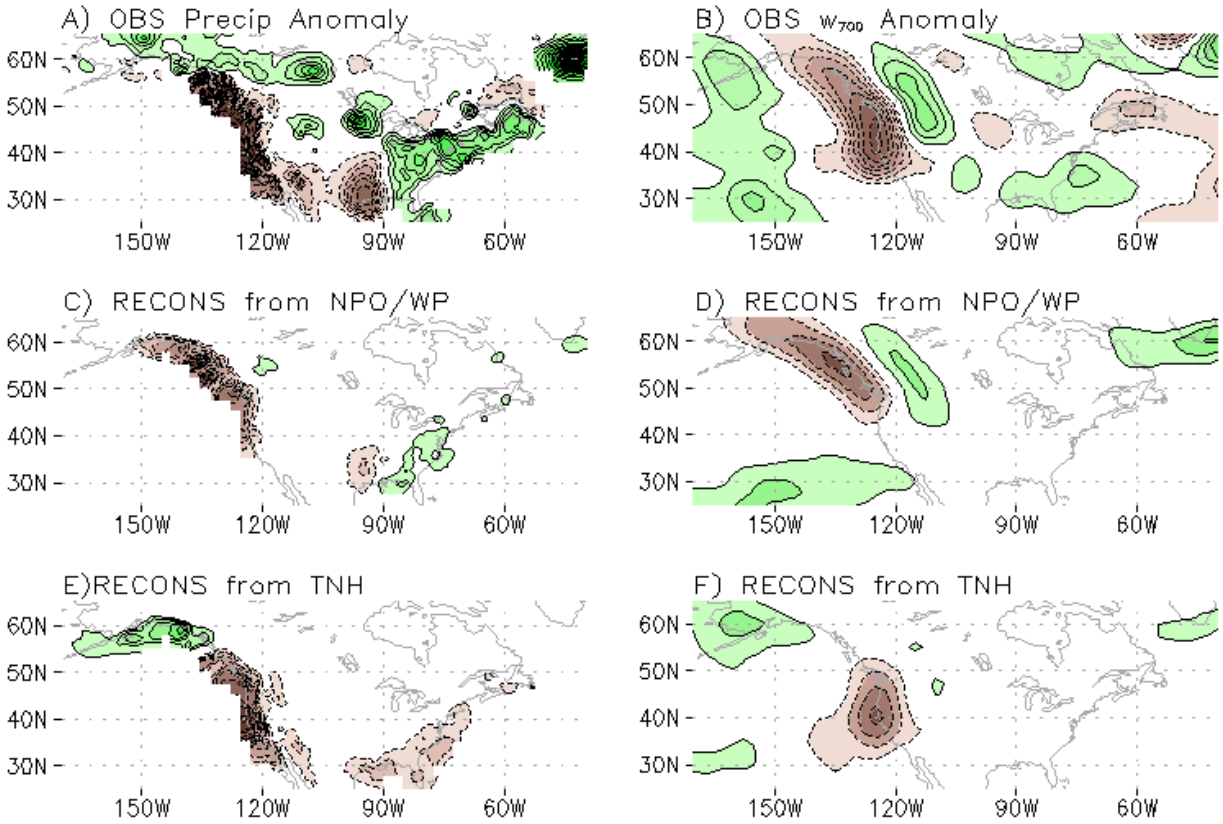

Figure 3. Precipitation and 700-hPa vertical velocity (W_{700}) anomalies during DJF2013-14: A) Observed precipitation anomaly, and its reconstruction from NPO/WP (C) and TNH (E) principal components. B) Observed W_{700} anomaly, and its reconstruction from the same principal components in D) and F), respectively. Contour interval and shading threshold is 0.25 mm/day for precipitation, and 1 cm/s for W_{700}.

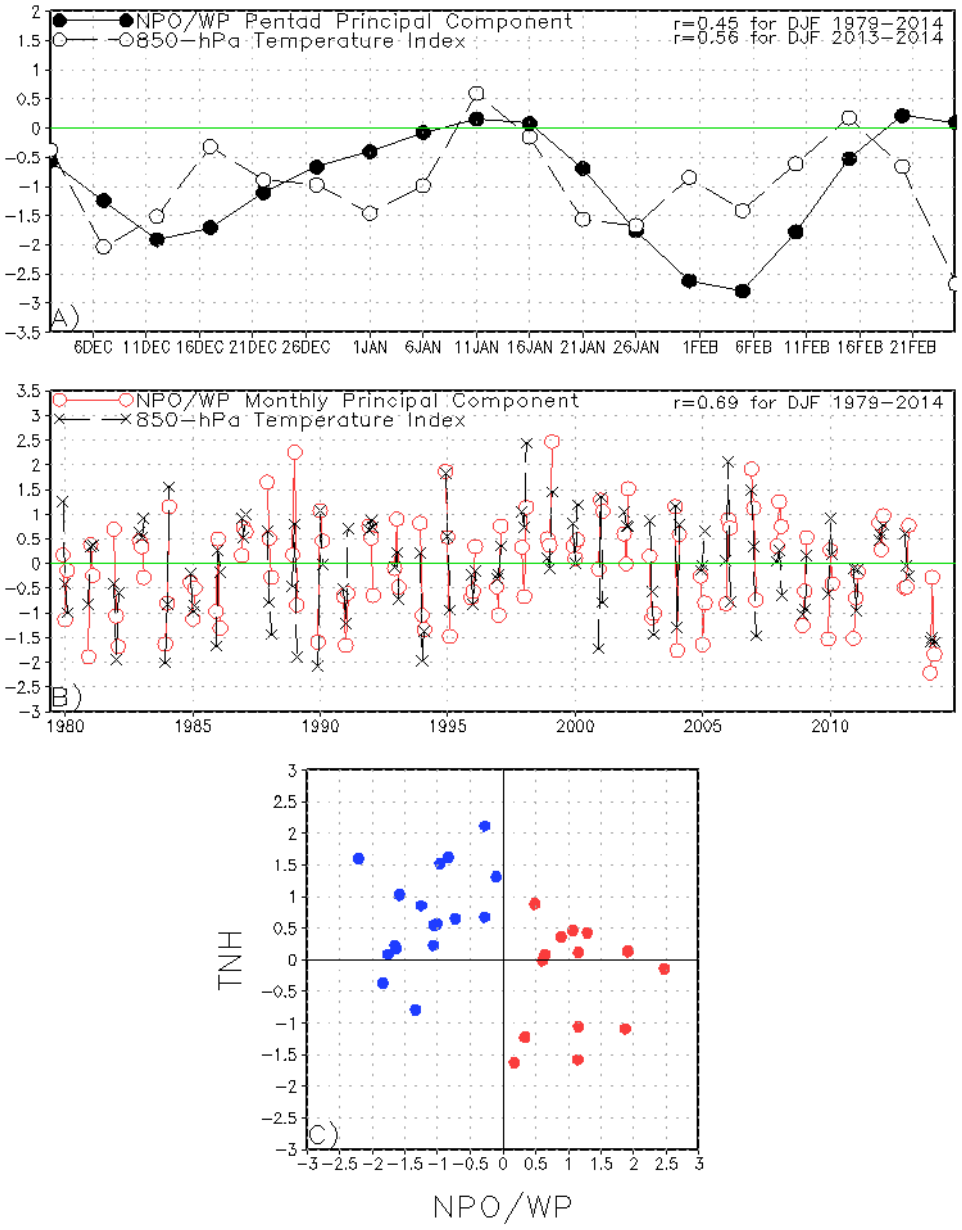

Figure 4. Pentad (A) and monthly (B) distribution of the NPO/WP principal component and T_{850} over the Great Plains (marked box in Fig. 1); the upper panel focuses on recent winter (DJF 2013-14) while the middle one covers the entire analysis period winters (1979-2014). The 200-hPa winter geopotential height (streamfunction) variability during 1979-2014 utilized for the seasonal (pentad) analysis, with correlation coefficients noted in the legend. (C) Scatter plot of the NPO/WP and TNH principal components from the 1979-2014 monthly analysis, when the T_{850} anomaly over the Great Plains exceed ±1 standard deviation. Blue (red) dots denote cold (warm) winter months.

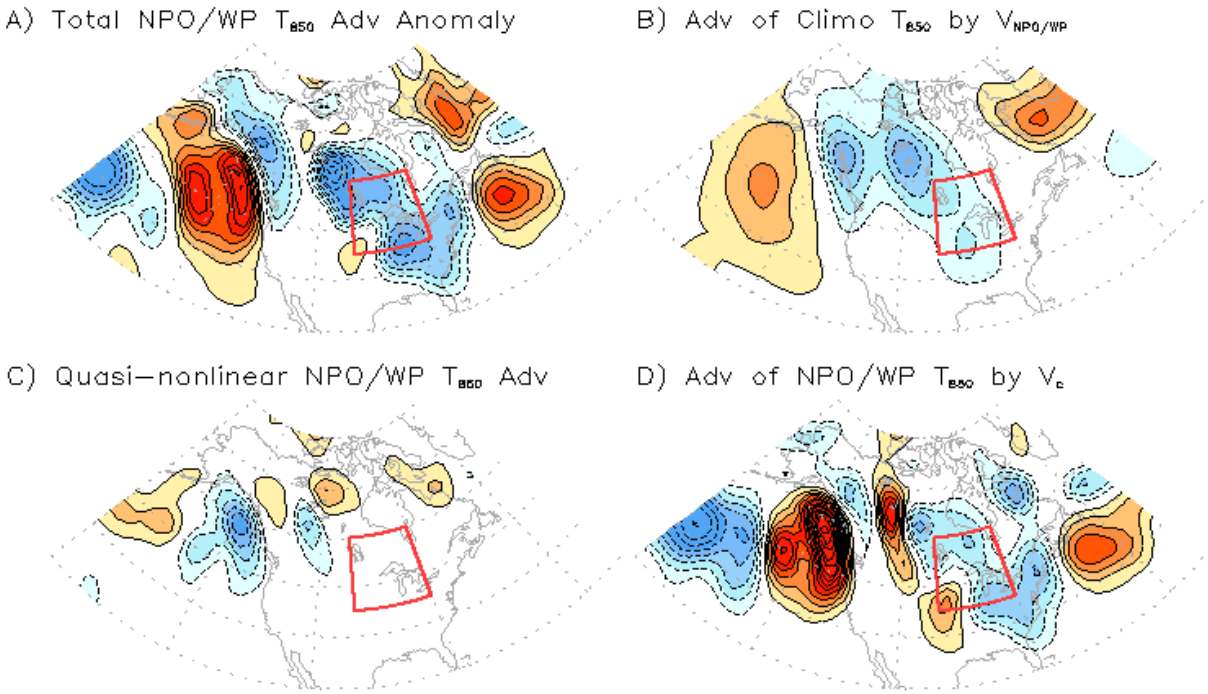

Figure 5. Reconstructed 850-hPa thermal advection related to NPO/WP. (A) Total thermal advection constituting the sum of panels *b*-*d*. (B) Advection of climatological 850-hPa temperature by the NPO/WP related wind anomaly, i.e., $\{-\overrightarrow{V_a} \bullet \vec{\nabla} T_c\}_{850\,\mathrm{hPa}}$, where $\overrightarrow{V_a}$ is the anomaly attributed to the NPO/WP and T_c is the climatological temperature. (C) Quasi-nonlinear term, $\{-\overrightarrow{V_a} \bullet \vec{\nabla} T_{NPO/WP}\}_{850\,\mathrm{hPa}}$, where $\vec{\nabla} T_{NPO/WP}$ is derived from panel (B) using a 3-day thermal dissipation time scale (cf. Lau 1979, Table 1). (D) The advection of $T_{NPO/WP}$ by the climatological 850-hPa wind, $\{-\overrightarrow{V_c} \bullet \vec{\nabla} T_{NPO/WP}\}_{850\,\mathrm{hPa}}$. Contour interval and shading threshold is 3.86E-6 K/s, a value that yields ΔT=1.0K for a 3-day thermal dissipation time scale. Data are also subject to a nine-point smoother to improve figure clarity.